

The $^{48}\text{Ca}(d,n)^{49}\text{Sc}$ Reaction at $E_d=20$ MeV
 Y. Iwasaki, D. Weber, and A. Galonsky

Neutron single particle states in nuclei have been studied by the (d,p) reaction. The (d,n) reaction is the isobaric mirror reaction to the (d,p) and is similar to it in reaction mechanism, but it has not generally been used for the study of proton single particle states because of the difficulty of neutron detection with high resolution. Instead, proton single particle states have been studied by the ($^3\text{He},d$) reaction, while its isobaric mirror reaction (t,d) has not generally been used for the study of proton single particle states because of the problems associated with accelerating particles out of a radioactive gas. Thus, there is a clear asymmetry between the situations regarding neutron and proton single particle states. It is neither necessary nor possible to remove the asymmetry. It is always desirable, however, to check the mechanism of a reaction that is extensively used for spectroscopy by comparing it with other reactions. The present work was undertaken to obtain (d,n) reaction data that can be used to check the ($^3\text{He},d$) reaction for a typical case.

It is expected that the spectroscopic factors derived from (d,n) and ($^3\text{He},d$) data agree with one another better for doubly magic target nuclei than for others. The $^{48}\text{Ca}(d,n)^{49}\text{Sc}$ reaction was chosen as the most favorable case from the point of view of experimental feasibility. The final nucleus ^{49}Sc has a series of well separated single proton states up to an excitation energy of about 7 MeV. The large positive Q value (7.394 MeV) removes the problem of the most prevalent contaminants, ^{12}C and ^{16}O . The $^{48}\text{Ca}(d,n)^{49}\text{Sc}$ reaction was studied previously at $E_d=5.5$ and 6.0 MeV.¹ At those low energies, however, peaks from ^{19}F and other contaminants were found in the region of $^{48}\text{Ca}(d,n)$ peaks, and the $l=3$ transfer to the $1f_{7/2}$ and $1f_{5/2}$ orbitals was relatively weak. Absolute cross sections were not reported. In recent work on the $^{86,87,88}\text{Ar}(d,n)^{87,88,89}\text{Y}$ reactions at $E_d=12$ MeV,² and the $^{56}\text{Fe}(d,n)^{57}\text{Co}$ reaction at $E_d=6.0, 8.0,$ and 10.0 MeV,³ derived spectroscopic factors were compared with those from ($^3\text{He},d$) data.

The present experiment is being performed with the neutron time-of-flight facility of the MSU cyclotron, using a 20 MeV deuteron beam. The length of the neutron flight path is 34 m. Only one out of three consecutive beam bursts is transported to the target to observe levels up to an excitation energy of about 7 MeV in ^{49}Sc . Neutrons are detected by a large liquid scintillation detector.⁴ The ^{48}Ca target is a self-supporting metallic foil with a thickness of 1 mg/cm². Fig. 1 shows the time-of-flight spectrum at 20° lab. The time resolution defined as the FWHM of the gamma ray peak is 0.93 ns. The FWHM of neutron peaks is about 120 keV or smaller. Angular distribution measurement is underway.

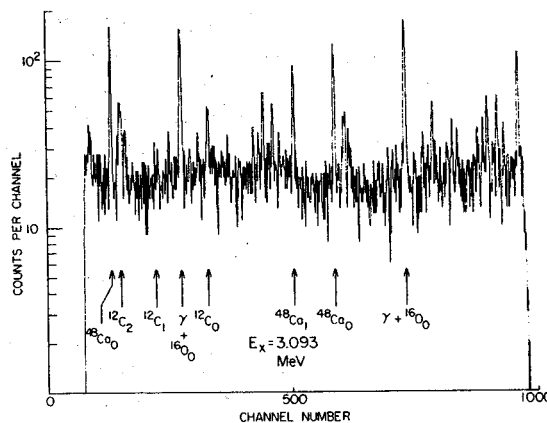


Fig. 1. Double time-of-flight spectrum at 20° lab. The collected charge is 1000 μC . For example, $^{48}\text{Ca}_1$ stands for $^{48}\text{Ca}(d,n_1)^{49}\text{Sc}$.

1. T.B. Grandy, W.J. McDonald, W.K. Dawson, and G.C. Neilson, Nucl. Phys. **A113** (1968) 353.
2. J.L. Horton and C.E. Hollandsworth, Phys. Rev. C **13** (1976) 2212.
3. A. Adam, O. Bersillon, and S. Joly, Phys. Rev. C **14** (1976) 92.
4. R.K. Bhowmik, R.R. Doering, L.E. Young, S.M. Austin, A. Galonsky, and S.D. Schery, Annual Reports 1974-75, 1975-76, Cyclotron Laboratory, Michigan State University, p. 120; Nucl. Instr. Meth. **143** (1977) 63.

The Observation of the $1g_{9/2}$ Deep-Hole States Near the $N=82$ Neutron Shell
 Via the $(^3\text{He}, \alpha)$ Reaction at 70 MeV on $^{124,130}\text{Te}$ and ^{144}Sm
 S. Gales, G.M. Crawley, D. Weber, and B. Zwieglinski

In the past few years a number of experiments have been carried out in order to study the location and the fragmentation of the $1g_{9/2}$ inner neutron hole strengths in the Sn isotopes.¹⁻³ A broad bump has been observed near 5 MeV excitation energy in these nuclei and recent high resolution studies⁴⁻⁵ have evidenced an underlying fine structure in this energy range in the $^{111,115,119}\text{Sn}$ isotopes. Therefore, it would be interesting to search for similar phenomena in neighboring nuclei with neutron numbers near the $N=82$ neutron closed shell.

The reactions $^{124,130}\text{Te}(^3\text{He}, \alpha)^{123,129}\text{Te}$ and $^{144}\text{Sm}(^3\text{He}, \alpha)^{143}\text{Sm}$ have been investigated at 70 MeV incident energy. The experimental setup was identical to the one described in our report of the study of $T_{<}$ and $T_{>}$ components in the lead region. An energy resolution of 55 keV was achieved in this experiment for target thicknesses of about $500 \mu\text{g}/\text{cm}^2$. An energy range of 25 MeV was explored in order to also look for narrow states ($T_{>}$ hole-analog states) located at higher excitation energy (12-18 MeV) in the residual nuclei.

In the case of the Te isotopes, very little is known about the neutron hole fragmentation of the valence shell ($3s_{1/2}$, $2d_{3/2}$, $1g_{7/2}$, $2d_{5/2}$, and $1h_{11/2}$). A typical spectrum from the $^{130}\text{Te}(^3\text{He}, \alpha)^{129}\text{Te}$ reaction recorded at a lab angle of 8° is shown in Fig. 1. A large number (≈ 20)

of discrete levels are observed up to 4 MeV excitation energy, most of which were previously unknown. The $(^3\text{He}, \alpha)$ reaction populates strongly $\ell=5$ and $\ell=4$ transitions assigned here as the components of the $1h_{11/2}$ and $1g_{7/2}$ neutron subshells in ^{129}Te . Above 4 MeV excitation energy a rather large enhancement of the cross-section is clearly observed between 4.5 and 10 MeV excitation energy. The mean energy and total width of this gross structure are 6.5 ± 0.5 and 4 ± 0.5 MeV, respectively. Very little fine structure is observed in this case which is consistent with the rather large width of the gross structure. The investigation of such simple modes of excitation of the nucleus was extended to a nucleus with a closed sdhg shell, namely ^{144}Sm . Going from ^{130}Te to ^{144}Sm there is a large increase in the proton number (52 to 62) and a rather small change in the neutron number (78 to 82). If the observation of this gross structure is due primarily to a neutron hole excitation, one would expect a small change in the excitation energy of the "giant resonance" like structure. The width resulting from the coupling to the more complicated states ($2p$ - $1h$, etc.) should however be affected by the closure of the neutron shell and the different proton distributions in the two nuclei. The spectrum from the $^{144}\text{Sm}(^3\text{He}, \alpha)^{143}\text{Sm}$ reaction recorded at a lab angle of 7° is shown in Fig. 2. Previous

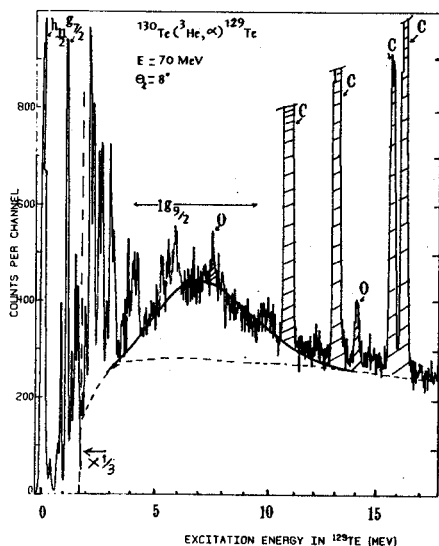


Fig. 1

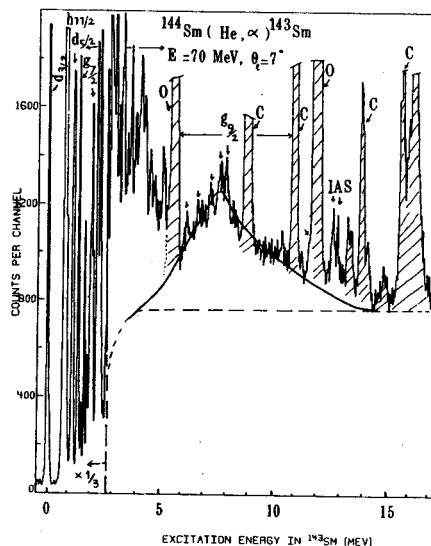


Fig. 2

studies of neutron pickup have established a large fragmentation of the $d_{5/2}$ and $g_{7/2}$ hole strength in this nucleus.⁶ Our preliminary analysis confirms these results. However, for the valence shell (sdhg) a clustering of new $l=5$ and $l=4$ transitions is observed between 3.5 and 5 MeV excitation energy. These new levels could account for the missing $l=4$, $g_{7/2}$ strength. The neutron hole excitation of deeper orbitals ($1g_{9/2}$) is clearly observed as a gross structure around 7.2 ± 0.5 MeV with a rather narrow width (2.4 ± 0.4 MeV) as compared to the Te case (4 ± 0.5 MeV). More fine structure seems to be present than in the previous case, although it seems difficult to extract angular distributions for individual groups in this case. In the tail of this broad structure, around 11.5 MeV excitation energy, the neutron hole-analog states are also populated (see Fig. 2). Additional data will be taken to search for narrow states around 18 MeV excitation energy where the T_1 components of the $1g_{9/2}$ inner hole strength are expected.

-
1. M. Sakai et al., Phys. Lett. 51B (1976) 51.
 2. S.Y. Van der Werf et al., Phys. Rev. Lett. 33 (1976) 712.
 3. E. Gerlic et al., Phys. Lett. 57B (1975) 338.
 4. G. Berrier-Ronsin et al., Phys. Lett. 67B (1977) 16.
 5. G. Berrier-Ronsin, G. Duhamel, S. Gales, E. Gerlic, E. Hourani, H. Langevin-Joliot, J. Van de Wiele, and M. Vergnes (to be published).
 6. G. Berrier, M. Vergnes, G. Rotbard, and J. Kalifa, Le Journal de Physique 37 (1976) 311, and references herein.

The Study of the $T_<$ and $T_>$ Components of Inner Hole States in the
Lead Region by Means of the $(^3\text{He}, \alpha)$ Reaction

S. Gales, G.M. Crawley, D. Weber, and B. Zwiaglinski

Most of the available data on the location and fragmentation of the neutron hole strength in the $N=126$ mass region (Pb, Bi) involve a few well resolved states below 3.5 MeV excitation energy in the residual nuclei.¹⁻³ Only a few experiments have been performed in order to investigate neutron pickup from the inner-shells in these nuclei.⁴⁻⁵ The present study of the reactions $^{208}\text{Pb}(^3\text{He}, \alpha)^{207}\text{Pb}$ and $^{209}\text{Bi}(^3\text{He}, \alpha)^{208}\text{Bi}$ was motivated mainly by the previous observation⁴⁻⁵ of a broad bump near 8 MeV excitation energy in ^{207}Pb . This enhanced part of the cross-section was tentatively interpreted as arising from the $1h_{11/2}$ inner neutron pickup. In order to investigate this phenomenon in more detail, the 70 MeV ^3He beam from the Michigan State University cyclotron was used to bombard 1 mg/cm² thick ^{208}Pb and ^{209}Bi targets. The α particles were detected in the focal plane of the Enge spectrograph using a 50 cm delay line gas counter.⁶ An energy resolution of 65 keV was achieved and an excitation energy range of 28 MeV was explored in the residual nuclei. Additional data were taken using thicker targets (5 to 10 mg/cm²) in order to emphasize the "giant resonance" like structure expected at high energy excitation (7 to 15 MeV) which characterize the population of the deeply-bound states in the lead region. The resulting spectrum for the $^{208}\text{Pb}(^3\text{He}, \alpha)^{207}\text{Pb}$ reaction is presented in Fig. 1. This spectrum clearly demonstrates

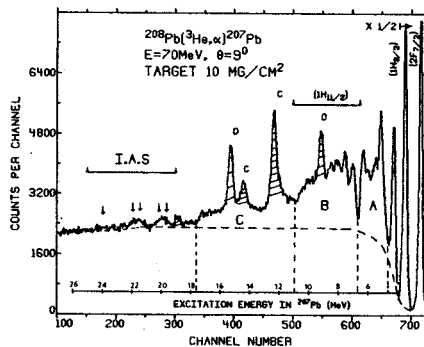


Fig. 1

the excitation of gross structures around 5.5 (region A), 8.5 (region B), and 14 MeV (region C), respectively. A careful investigation of the high energy part of this spectrum shows that the $T_>$ components of the deep-hole states are also observed in ^{207}Pb .⁷

Due to the good energy resolution and to the large range of excitation energy explored in

the present work, a detailed study has been carried out for the low-lying states (discrete levels up to 4.5 MeV in ^{207}Pb) as well as for the gross structure observed at higher energy. The DWBA analysis gives quite good agreement with the experimental data for the first few excited states of known ℓ values in ^{207}Pb . The missing $2f_{7/2}$, $1h_{9/2}$, and $1i_{13/2}$ neutron hole strength has been located in some narrow peaks between 4.5 and 6.7 MeV excitation energy in ^{207}Pb . A broad structure was observed in previous work^{4,5} around 8.3 MeV in ^{207}Pb , and in the present case a number of narrow states have been observed up to 9.6 MeV showing that fine structure is still observable at these excitation energies. The angular distributions of the individual groups (region B of Fig. 2) as well as the one extracted for the whole bump are consistent with an $\ell=5$ angular momentum transfer. About 70% of the $1h_{11/2}$ inner neutron hole strength has been located between 6.7 and 10.5 MeV in ^{207}Pb . A new broad peak is observed around 14 MeV excitation energy in ^{207}Pb . This large structure is tentatively interpreted as due to neutron pickup from the next major shell, viz. $1g_{9/2}$. The deduced centroid energies for both $T_>$ and $T_<$ components of the neutron hole strength are presented in Table I and compared with previous results.

The influence of the coupling of the proton with the neutron hole states is now being investigated using the $^{209}\text{Bi}(^3\text{He}, \alpha)^{208}\text{Bi}$ reaction. The measured spectra are very similar to those from ^{207}Pb , although less fine structure is observable due to the multiplet nature of the residual states in ^{208}Bi .

Finally, the deduced strengths of the hole-analog configuration in ^{207}Pb are in reasonable agreement with those of their parent states in ^{207}Tl only if the Lane coupled-channel equation is used to deduce the form factor of these deeply-bound states.

1. G.R. Satchler, W.C. Parkinson, and D.L. Hendrie, Phys. Rev. **187** (1969) 1491.
2. G.M. Crawley, E. Kashy, W. Lanford, and H.G. Blosser, Phys. Rev. C **8** (1973) 2477.
3. M.R. Smorak, Nucl. Data **B22** (1977) 487.
4. M.B. Lewis, Phys. Rev. C **11** (1975) 145.
5. J. Van de Wiele, E. Gerlic, M. Langevin-Joliot, and G. Duhamel, Nucl. Phys. **A297** (1978) 61.
6. R.G. Markham and R.G.H. Robertson, Nucl. Inst. and Meth. **129** (1975) 131.
7. S. Gales, G.M. Crawley, D. Weber, and B. Zwiaglinski, Phys. Rev. Lett. **41** (1978) 292.

Table I. Centroid energies and experimental widths of neutron hole states in ^{207}Pb .

Neutron orbital	$\bar{E}_<(j)$ (MeV)	$\bar{E}_>(j)$ (MeV)	\bar{E}_j (MeV) b)	Γ_j exp (MeV) c)	Γ_j (MeV) b)
$3p_{1/2}$	0.00		0.00		
$2f_{5/2}$	0.57	--	0.60		
$3p_{3/2}$	0.90	--	0.90		
$1i_{13/2}$	1.87	--	1.60		
$2f_{7/2}$	2.92	--	2.30		
$1h_{9/2}$	4.01	--	3.40		
$3s_{1/2}$	(7.3)	19.31	5.7		1.8
$2d_{3/2}$	(7.6)	19.69	5.7		1.8
$1h_{11/2}$	8.5	20.65	8.3 ± 1	3.7 ± 0.2	3.7
$2d_{5/2}$	(9.0)	21.00	6.8		2.5
$1g_{7/2}$	(10.8)	22.89	10.7		5.8
$1g_{9/2}$	≈ 14.0		14.0	5.1 ± 0.5	10

- a) Centroid energy of the $T_<$ component of neutron hole states (j) in ^{207}Pb . The numbers listed in parentheses are not deduced from this analysis. These numbers were obtained by using the relation $E_<(j) = E_>(j) - \Delta E(T_>-T_<)$ where $E_>(j)$ is the excitation energy of the hole analog configuration⁷ and $\Delta E(T_>-T_<)$ is taken equal to 12 MeV from the known values for the $h_{11/2}$ orbital.
- b) The centroid energies listed in this column are from Ref. 1 for the $3p_{1/2}$, $2f_{5/2}$, $3p_{3/2}$, $2f_{7/2}$ and $1h_{9/2}$ orbitals and from Ref. 4 from the more deeply-bound holes ($3s_{1/2}$ to $1g_{9/2}$). The width of these inner hole states are also from Ref. 4.
- c) Experimental widths deduced from this work for the hole strength distribution of the $1h_{11/2}$ and $1g_{9/2}$ orbitals.

Damping of Single-Particle Motion
and Giant Resonances

G. Bertsch, R. Broglia, and G. Richter

We compute the spreading of simple modes of nuclear excitation in a model where the simple states couple to particle-hole excitations of the core. Both particle-particle correlations and particle-hole correlations are included in the model of the excitations, by using RPA Green's functions to describe the excitation of the core. We find that inclusion of the correlations increases the damping of excitations in the range 5-15 MeV by an order of magnitude. Nevertheless, both single-particle and collective state damping are predicted to be somewhat less than is found empirically. Of the two kinds of correlations, the particle-hole seems more important than the particle-particle. In the damping of giant resonances, there is a significant interference effect which reduces the damping width to below that of a single-particle at an equivalent excitation energy.

The (p, t_0) Angular Distribution with Deep Minima and the Zero-Range DWBA Calculation
 Y. Iwasaki, E. Kashy, and R.G. Markham

The experimental angular distribution for the ground state transition in the (p, t) reaction on an even-even target nucleus has unique features which can be summarized as follows:

- (1) It is a rapidly changing function of the reaction angle, having sharp peaks and especially deep minima.
- (2) It is a very slowly varying function of the target mass number and charge at a fixed incident energy, and depends smoothly on the incident energy.

Experiments of the (p, t) reaction were performed generally with angular steps of 3° to 5° . Therefore the angular positions and the depths of the minima of the experimental (p, t_0) angular distribution were not known very accurately. We have measured angular distributions for the transitions $^{54}\text{Fe}(p, t_0)^{52}\text{Fe}$ and $^{50}\text{Ti}(p, t_0)^{48}\text{Ti}$ with a step of 1.0° in general, and with a step of 0.5° around some of the deep minima. A quintuplet of slits was placed at the entrance to the Enge split-pole magnetic spectrograph. Neighboring slits were separated by 1.0° and the width of each slit was 0.5° in one case and 0.33° in another. The delay-line counter¹ was placed a little forward of the focal plane. Particles reaching the counter and not corresponding to the (p, t_0) transition were easily rejected by using time-of-flight signals and energy-loss signals. Thus, measurement was made at five consecutive angles at the same time. Figs. 1 and 2 show the measured angular distributions.

The above features (1) and (2) suggest that the experimental (p, t_0) angular distribution possibly contains information about geometrical properties of the nucleus such as nuclear radius or surface diffuseness. However, analysis of the experimental angular distribution is extremely difficult because of the constitution of the existing theory. The only practical theory of the (p, t) reaction is the distorted-wave Born approximation (DWBA) theory. Almost all practical analyses of experimental data were performed by the zero-range DWBA theory. It was successful in reproducing overall qualitative features of the angular distribution. In no case, however, was a completely exact reproduction of all the data points possible. The angular distribution calculated by the zero-range DWBA theory depends upon a large number of parameters of the neutron-binding potential and the optical potentials in the entrance and exit channels. There has been no attempt to seek a best fit to the experimental angular distribution by a variation of the parameters. The common practice found in the

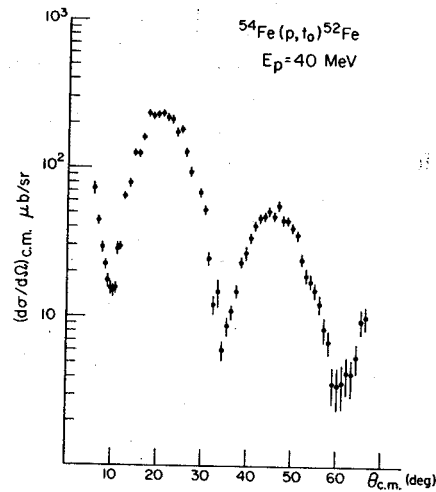


Fig. 1

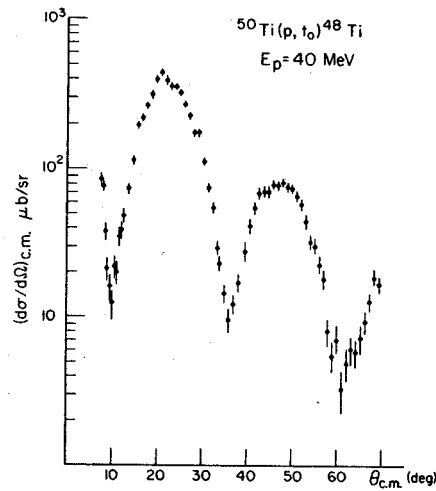


Fig. 2

literature is to try some several sets of optical potentials determined by proton and triton elastic scattering data or derived from some sources and to choose the set that gives a best overall fit to the data. This procedure originates probably from the common belief that the optical potentials used in the DWBA calculation of a transfer reaction should reproduce elastic scattering cross sections. However, there are wellknown ambiguities in determination of the optical potential by a best fit to elastic scattering data. One of the ambiguities is a continuous ambiguity concerning the well-depth V and the radius parameter r_0 of the real central part. Potentials having different sets of values of V and r_0 give almost equally good fits to elastic scattering differential cross sections, if Vr_0^n is kept constant where $n=2$. Since V and r_0 are not independently

significant, there arises a motive to fix either one of them, and the common practice is to fix r_0 leading to the introduction of fixed-geometry optical potentials.^{2,3,4} The common use of fixed-geometry optical potentials in the DWBA calculation of a transfer reaction assumes implicitly that the Vr_0^n ambiguity exists in the case of a transfer reaction just as in the case of elastic scattering. However, this is by no means true. By choosing an appropriate pair of values for V and r_0 , while keeping Vr_0^n ($n \approx 2$) constant, an improvement in the fit to the experimental (p, t_0) angular distribution is achieved without losing a good fit to the elastic scattering angular distribution. Even with this procedure a very good fit to the (p, t_0) angular distribution is not generally achieved. However, there is no reason to believe that the optical potentials that should be used in the DWBA calculation of a transfer reaction are exactly those that reproduce completely the elastic scattering data. Elastic scattering is coupled with a number of reaction channels, and various higher order processes contribute to experimental elastic scattering cross sections. The optical potential that should be used to generate the one-body distorted wave function in the entrance or exit channel of a transfer reaction does not in general reproduce elastic scattering cross sections completely.⁵ Therefore it is possible to take a point of view different from the conventional one. We are trying to get as good a fit as possible to the experimental (p, t_0) angular distribution varying geometrical parameters as well as well-depth parameters. Stated in another way, the problem is to ask if there is a solution (i.e. a set of potential parameters) that gives a complete fit to the experimental (p, t_0) angular distribution within the framework of the zero-range DWBA theory, and to ask to what extent the solution is unique. In

order to get an idea about the uniqueness, it is necessary to know the general dependence of the calculated (p, t_0) angular distribution on each of the potential parameters. Therefore, a very extensive series of DWBA calculations was performed with the zero-range DWBA code DWUCK⁶ for ^{54}Fe , ^{50}Ti , and ^{46}Ti targets. A set of the neutron-binding potential and the optical potentials of the entrance and exit channels⁷ was chosen as a standard, and every parameter was changed over a reasonably wide range so as to show a general trend. Further, cooperative effects of two or more parameters were studied, changing the parameters in a correlated manner when it seemed physically meaningful. After having studied the general trend of dependence on all the parameters, we are now seeking a best fit to the experimental (p, t_0) angular distribution. The calculated angular distribution is very sensitive to the geometrical parameters. It seems that there is only a narrow choice for the geometrical parameters to give a very good fit to the experimental angular distribution. It is important to see if the values of the parameters are consistent with information derived from other sources, e.g. charge distribution radius and diffuseness.

-
1. R.G. Markham and R.G.H. Robertson, MSUCL-173 (1975).
 2. F.G. Perey, Phys. Rev. 131 (1963) 745.
 3. F.D. Becchetti, Jr. and G.W. Greenlees, Phys. Rev. 182 (1969) 1190.
 4. E.R. Flynn, D.D. Armstrong, J.G. Beery, and A.G. Blair, Phys. Rev. 182 (1969) 1113.
 5. L.R. Scherk and W.R. Falk, Nucl. Phys. A183 (1972) 240.
 6. P.D. Kunz, University of Colorado (unpublished).
 7. H. Nann and B.H. Wildenthal, Phys. Rev. C 13 (1976) 1009; P. Decowski, W. Benenson, B.A. Brown, and H. Nann, MSUCL-232 (1976).

The angular distribution for a transfer reaction calculated by the zero-range distorted-wave Born approximation (DWBA) theory depends on a large number of parameters of the optical potentials in the entrance and exit channels as well as of the potential that binds the transferred particle(s). To be specific, we consider the ground state transition in the (p,t) reaction on an even-even target nucleus. A very extensive series of computer experiments was performed using the zero-range DWBA code DWUCK¹ to study the behavior of the calculated (p,t_0) angular distribution as a function of the parameters. Some general phenomena were discovered during the course of the computer experiments and were confirmed by further series of calculations. We summarize them in the following:

The continuous ambiguity of the type Vr_0^n ($n=2$) does not persist in the calculation of the (p,t_0) angular distribution. Fig. 1 illustrates how the calculated angular distribution changes with a variation of V and r_0 of the proton optical potential keeping Vr_0^2 constant. The angular positions of the maxima are remarkably constant. The peaks in the angular distribution move toward smaller angles with increasing r_0 . The corresponding decrease in V acts to move back the peaks to the original angular positions but changes further the shape of the angular distribution. Fig. 2 shows clearly that there is no Vr_0^n ambiguity for the triton optical potential. Fig. 3 indicates, however, that the situation for the triton optical potential is characteristically different from that for the proton optical potential. The change in the angular distribution shape in Fig. 2 is brought about almost totally by the change in r_0 , the change in V having only a very small effect.

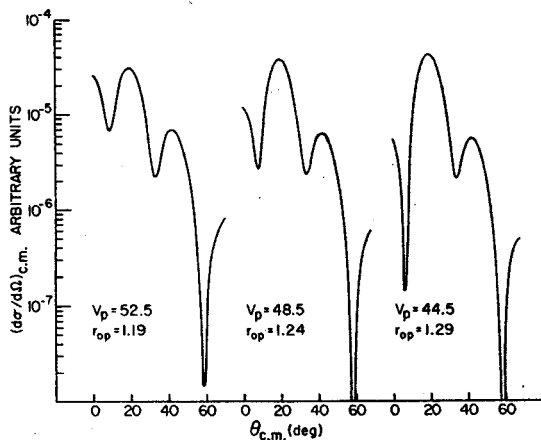


Fig. 1. Angular distributions calculated by DWUCK for $^{54}\text{Fe}(p,t_0)^{52}\text{Fe}$. The parameters not indicated in the figure have the values of Ref. 2. The same is true for Figs. 2 and 3.

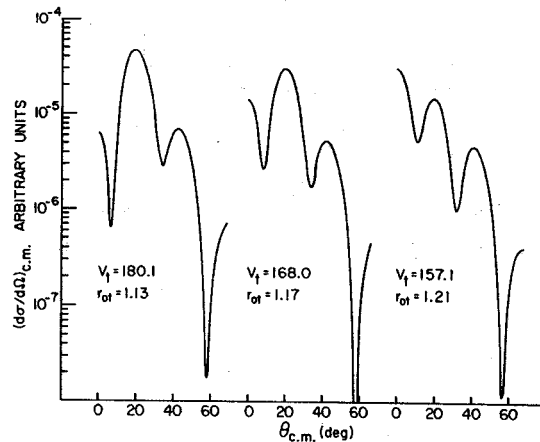


Fig. 2

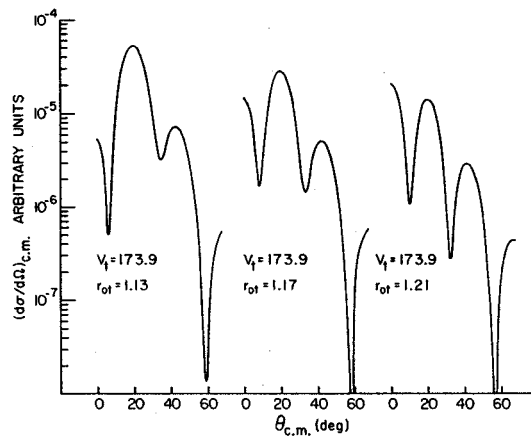


Fig. 3

The character of the role of the triton optical potential is determined by the relation between the radius parameter r_{ot} of the real part of the triton optical potential and the radius parameter $r_{F.F.}$ of the form-factor-generating potential that binds the transferred neutrons.

If $r_{ot} < r_{F.F.} - 0.5$ (fm), the calculated angular distribution is quite insensitive to the well depth of the real part of the triton optical potential. If $r_{ot} > r_{F.F.} + 0.5$ (fm), the dependence of the calculated angular distribution on the real well depth and r_{ot} is qualitatively the same as that on the well depth and radius parameters of the real central part of the proton optical potential. The region $r_{F.F.} - 0.5 \leq r_{ot} \leq r_{F.F.} + 0.5$ is a transitional region, where the dependence of the calculated angular distribution on the triton real well depth and r_{ot} is a little more complicated than in the above two regions. The above

general effect was confirmed for $r_{F.F.} = 1.15, 1.25,$ and 1.35 fm, and for ^{54}Fe , ^{50}Ti , and ^{46}Ti targets, and for surface-absorption and Becchetti-Greenlees proton optical potentials. There was no exceptional case.

Further study is going on. It seems to indicate that the above results can be generalized to any strong volume-absorption optical potential instead of the triton optical potential, and to any surface-absorption or almost surface-absorption potential instead of the proton optical potential. A full account of the present work will be published in the near future.

-
1. P.D. Kunz, University of Colorado (unpublished).
 2. H. Nann and B.H. Wildenthal, Phys. Rev. C **13** (1976) 1009; P. Decowski, W. Benenson, B.A. Brown, and H. Nann, MSUCL-232 (1976).

The $^{65}\text{Cu}(p,t)^{63}\text{Cu}$ Reaction

Y. Iwasaki, G.M. Crawley, R.G. Markham, J.E. Finck, and J.H. Kim

The $^{65}\text{Cu}(p,t)^{63}\text{Cu}$ reaction was studied previously at $E_p=18.0$ and 19.5 MeV¹ and at $E_p=51.9$ MeV.² The study at 51.9 MeV focused on low-lying particle-core-coupled states in ^{63}Cu and pointed out the usefulness of the (p,t) reaction for a study of the core-excited component of a particle-core-coupled state.² The data at 19.5 MeV concerning the low-lying states were analyzed quantitatively in terms of the particle-core wave functions.¹

The present experiment at $E_p=40$ MeV extends the range of a high-resolution study of the $^{65}\text{Cu}(p,t)^{63}\text{Cu}$ reaction up to a region of higher excitation energies so far not studied. The target was a self-supporting metallic foil with a thickness of $250 \mu\text{g}/\text{cm}^2$. Tritons were detected by a delay-line counter³ placed at the focal plane of the Enge split-pole magnetic spectrograph. The overall energy resolution was 16 keV. Other kinds of particles reaching the detector were excluded by use of time-of-flight and energy loss signals. Angular distributions were obtained for 34 transitions to levels in ^{63}Cu up to an excitation energy of 3.8 MeV. Assignment of the transferred angular momentum L was made to most of the transitions by the phenomenological systematics of angular distribution shape which was obtained from the $^{64}\text{Ni}(p,t)^{62}\text{Ni}$ reaction.⁴ The results are summarized in Table I. Fig. 1 shows angular distributions for some of the stronger transitions. A DWBA analysis is underway.

It is expected that a comparison of the present data with the (p,p') data at the same proton energy⁵ would serve for a better understanding of the particle-core coupling in ^{63}Cu .

Table I. Experimental results. The values of J^π are taken from Ref. 6.

E_x (MeV)	J^π	$(d\sigma/d\Omega)_{\text{max}}^{\text{cm}}$ ($\mu\text{b}/\text{sr}$)	$(\theta_{\text{max}}^{\text{cm}})$ (deg)	L
0.00	$3/2^-$	626	(20.6)	0
0.67	$1/2^-$	17.5	(9.3)	2
0.96	$5/2^-$	46.3	(9.3)	2
1.33	$7/2^-$	110	(9.3)	2
1.41	$5/2^-$	10.5	(9.3)	2
1.55	$3/2^-$	7.9	(18.1)	0+2
1.86	$7/2^-$	11.5	(6.2)	2
2.01	$3/2^-$	16.2	(6.2)	2
2.06	$1/2^-, 3/2^-$	22.7	(6.2)	2
2.09+(2.08)	$7/2^-, 5/2^-$	12.5	(6.2)	
2.21	$9/2^-$	11.7	(6.2)	4
2.34	$5/2^-$	22.4	(6.2)	4
2.41	$7/2^-$	2.2	(6.2)	
2.51		23.0	(6.2)	3
2.54	$5/2^-$	22.8	(6.2)	4
2.68		57.3	(6.2)	4
2.79		8.4	(6.2)	(0+2)
2.85		5.3	(6.2)	4
2.88		6.4	(6.2)	4
2.99		8.3	(6.2)	2
3.04		13.8	(6.2)	2
3.11		2.8	(6.2)	2
3.14		3.0	(9.3)	2
3.19		12.3	(9.3)	4
3.22		23.7	(6.2)	4
3.26		22.3	(6.2)	4
3.31		19.7	(6.2)	2
3.38		3.0	(6.2, 9.3)	4
3.44		6.3	(6.2)	
3.47		18.4	(6.2)	
3.58		26.3	(6.2)	0+2
3.68		19.2	(6.2)	4
3.72		19.7	(6.2)	(3)

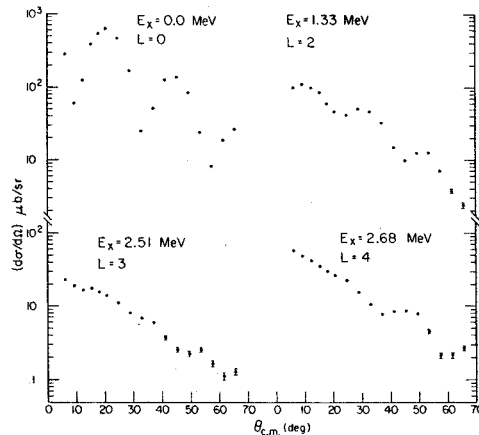


Fig. 1

1. R.G. Markham and H.W. Fulbright, Nucl. Phys. A203 (1973) 244.
2. Y. Iwasaki, M. Sekiguchi, F. Soga, and N. Takahashi, Phys. Rev. Lett. 29 (1972) 1528.
3. R.G. Markham and R.G.H. Robertson, MSUCL-173 (1975).
4. D.H. Kong-A-Siou and H. Nann, Phys. Rev. C 11 (1975) 1681.
5. Y. Iwasaki, G.M. Crawley, R.G. Markham, J.E. Finck, and J.H. Kim, Annual Report 1977-78, Cyclotron Laboratory, Michigan State University (present volume).
6. C.T. Papadopoulos, A.G. Hartas, P.A. Assimakopoulos, G. Andritsopoulos, and N.H. Gangas, Phys. Rev. C 15 (1977) 1987.

The broad structure observed in (p,t) reactions on the Sn isotopes has been tentatively identified as pickup of two neutrons from deep orbits in these nuclei. A letter reporting this work has been published.¹ Further work on this problem is taking place in the following directions.

To complete the series of Sn isotopes, the lightest stable Sn isotope ^{112}Sn was used as a target, and a broad bump was observed in the residual nucleus ^{110}Sn . The spectrum observed is shown in Fig. 1. The excitation energy of the gross structure followed the systematic trend of decreasing excitation energy with decreasing A of the target found previously. However, the width of the peak increased in ^{110}Sn to about 2.5 MeV, whereas the trend had been for the width to decrease from 2.7 MeV in ^{122}Sn to 1.9 MeV in ^{114}Sn .

A search of the fine structure observed in the light palladium and cadmium isotopes is also being made to see whether any 0^+ strength can be identified. Such states are of particular interest since they certainly correspond to two neutrons being picked up from the same orbit. A tentative 0^+ assignment has been made for a state in ^{104}Cd at an excitation energy near 6 MeV. The angular distribution for this state together with the ground state angular distribution is shown in Fig. 2. While the maxima and minima of the angular distributions for the excited states are not as pronounced as for the ground state, both angular distributions appear to be in phase.

Other series of isotopes including the cadmium and samarium isotopes are being studied to search for systematic trends in the behavior of the gross structure. Preliminary studies in $^{90,92}\text{Zr}$ indicate that a weak structure is observed at an excitation energy near 11 MeV in $^{88,90}\text{Zr}$ which may arise from pickup from the $f_{7/2}$ shell. This feature is much less pronounced than in the Sn isotopes.

Finally, a preliminary search has been made using 90 MeV protons from the Indiana University Cyclotron to see whether the structure is observable at higher proton energies. A peak corresponding to those observed at 42-45 MeV bombarding energy was observed in the reactions $^{124}\text{Sn}(p,t)$, $^{122}\text{Sn}(p,t)$, and $^{120}\text{Sn}(p,t)$, and some suggestions of peaks were observed in the $^{208}\text{Pb}(p,t)$ and $^{154}\text{Sm}(p,t)$ reaction. However, in these latter cases, better statistics are needed to confirm these observations. Another run will be made soon at IUCF.

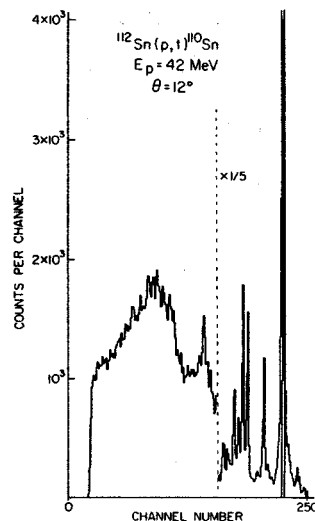


Fig. 1. Spectrum of tritons from the reaction $^{112}\text{Sn}(p,t)^{110}\text{Sn}$ at $E_p = 42$ MeV.

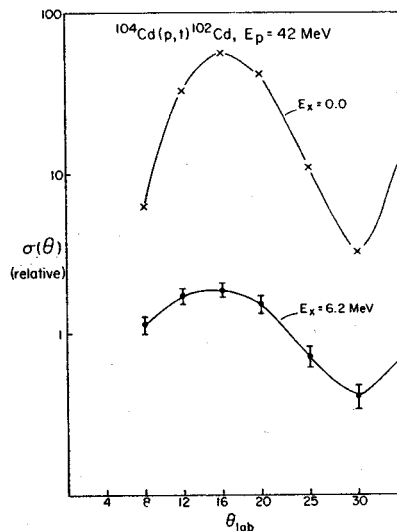


Fig. 2. Angular distributions for the ground state (0^+) and excited state at 6.2 MeV as observed in the $^{104}\text{Cd}(p,t)^{102}\text{Cd}$ reaction.

[†] On leave from the Institute of Nuclear Research, Warsaw, Poland.

1. G.M. Crawley, W. Benenson, D. Weber, and B. Zwięglinski, Phys. Rev. Lett. **39** (1977) 1451.

A considerable effort has been devoted¹ in the past towards the study of the T=3/2 states in ^{11}B and ^{11}C . However, only the analogs of the g.s., 0.320 MeV first excited and possibly the 1.785 MeV second excited state of the parent ^{11}Be have been identified¹ in ^{11}B . The recent shell-model calculations of Kurath et al² for the positive-parity states in mass 11 have considerably intensified the interest in the structure of these nuclei. In the present work the ^{11}B nucleus was investigated in the excitation energy range from 9.0 to 22.0 MeV with the $^9\text{Be}(^3\text{He},\text{p})^{11}\text{B}$ reaction at the bombarding energy $E(^3\text{He}) = 38$ MeV. Reaction products were momentum-analyzed with the Enge split-pole spectrograph and detected with the delay-line proportional counter at the spectrograph focal plane. A spectrum measured at $\theta_{\text{lab}} = 27.5^\circ$ is presented in Fig. 1 (upper spectrum). The spectrum is dominated by a strongly excited doublet at 14.55 MeV. Another outstanding feature is the excitation of narrow states at 16.44, 17.67, 19.09 and 21.17 MeV. The $(^3\text{He},\text{p})$ reaction may excite both T=1/2 and T=3/2 states in the final nucleus. To make unique isospin assignments the $^9\text{Be}(\alpha,\text{d})^{11}\text{B}$ reaction was studied in the excitation energy range from 14.2 MeV to 20.8 MeV. Assuming pure isospin, the latter reaction is expected to populate only

the T=1/2 part of the spectrum. The spectra of the $^9\text{Be}(\alpha,\text{d})^{11}\text{B}$ reaction presented in Fig. 1 demonstrate that the 14.56 MeV doublet has T=1/2, whereas the narrow states have T=3/2. The differences between the excitation energies of these narrow states and the excitation energy of the ^{11}Be ground state analog in ^{11}B suggest the following tentative correspondence with the levels¹ of the parent ^{11}Be - 16.44 MeV (3.96 MeV), 17.67 MeV (5.25 MeV), 19.09 MeV (6.72 MeV) and 21.17 MeV (8.84 MeV).

$^9\text{Be}(\alpha,\text{d})^{11}\text{B}$ experiments are presently underway to test the nature of the 21.17 MeV state and the group of states between 12.0 MeV and 14.2 MeV. Measurements of $^9\text{Be}(^3\text{He},\text{p})^{11}\text{B}$ angular distributions will be continued to make tentative spin-parity assignments for the states in question. In particular it is of considerable interest whether one or both members of the 14.56 MeV doublet can be interpreted as states belonging to the $(\text{d}_{5/2})^2_5^+$ configuration.

1. F. Ajzenberg-Selove, Nucl. Phys. A248 (1975) 1.
2. W.D. Teeters and D. Kurath, Nucl. Phys. A275 (1977) 61.

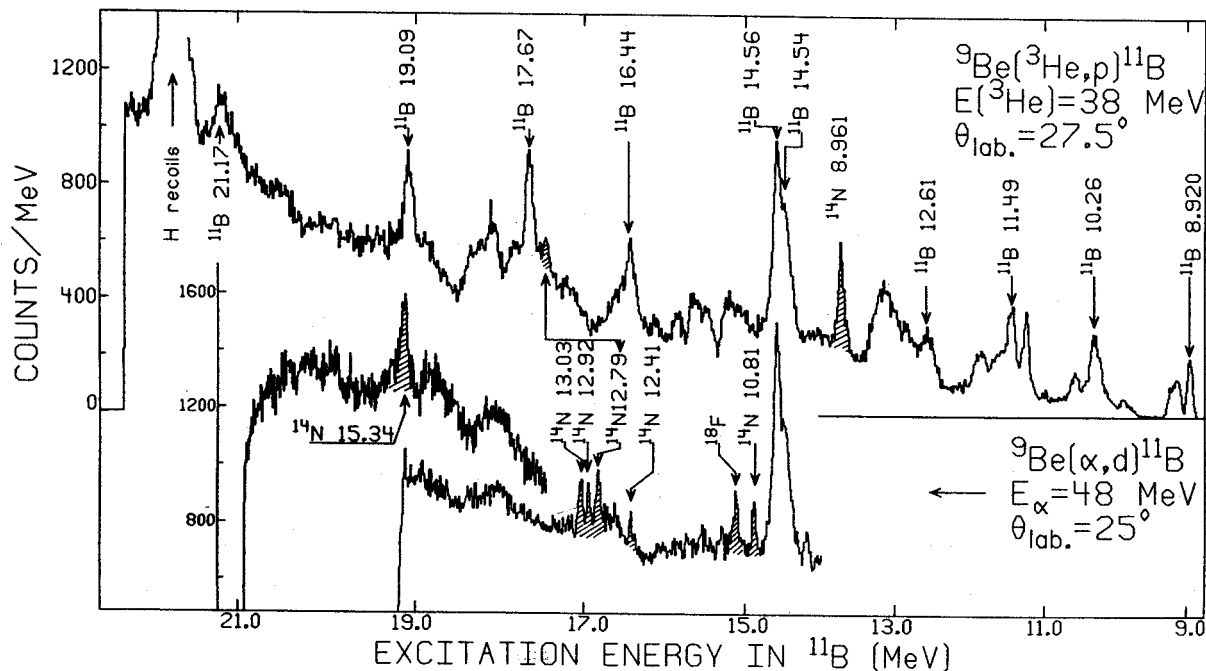


Fig. 1. The spectra of particles from $^9\text{Be}(^3\text{He},\text{p})^{11}\text{B}$ and $^9\text{Be}(\alpha,\text{d})^{11}\text{B}$ reactions.

The nuclei near ^{208}Pb are a useful testing ground for nuclear structure calculations. It is possible to test weak and intermediate coupling schemes as well as full shell model calculations. In comparing the predictions with the data, it is the high spin states in particular which are of great importance as a result of their simple configurations. Previous work¹ in the ^{40}Ca region has established that three nucleon transfer reactions preferentially populate high spin states and that distorted wave Born approximation (DWBA) calculations provide good fits to the data and show a high degree of spin selectivity. The level structure of the thallium nuclei is not well understood. In an effort to improve this understanding with particular emphasis upon the location of high spin states, the $^{208}\text{Pb}(p,\alpha)^{205}\text{Tl}$ and $^{206}\text{Pb}(p,\alpha)^{203}\text{Tl}$ reactions were performed at 35 MeV.

Isotopically enriched targets consisting of $100\ \mu\text{g}/\text{cm}^2$ ^{208}Pb and $150\ \mu\text{g}/\text{cm}^2$ ^{206}Pb evaporated onto $20\ \mu\text{g}/\text{cm}^2$ carbon foil backings were used. The reaction products were detected after analysis with an Enge Split pole spectrograph in a delay-line gas counter² backed by a plastic scintillator. A number of spectra were also recorded on photographic plates, together with spectra from the $^{93}\text{Nb}(p,\alpha)^{90}\text{Zr}$ reaction. The known Tl levels below 1 MeV excitation together with the known states of ^{90}Zr recorded on the emulsion were used to calibrate the Tl plate and counter spectra. Levels up to 4 MeV excitation were observed and their excitation energies were determined to ± 3 keV below 2 MeV excitation, ± 5 keV between 2 and 3 MeV excitation, and ± 8 keV above 3 MeV excitation. The resolution obtained was 15-25 keV (FWHM) for the plate spectra and 25-35 keV (FWHM) for the counter spectra. Preliminary results for ^{205}Tl were presented in last year's annual report.²

Two position spectra are shown for ^{203}Tl in Fig. 1. As the DWBA calculations discussed below indicate that high spin states peak at more backward angles than states having low spin, the large peaks above 2 MeV excitation which emerge at 40° are high spin states. Angular distributions are shown for ^{205}Tl , together with arbitrarily normalized DWBA calculations in Fig. 2. The calculations were performed with the code DWUCK⁴ using

cluster model form factors and the optical model parameters shown in Table I which were taken from $^{206,208}\text{Pb}(\alpha,p)$ studies.⁵ The quality of the fits is excellent. While the angular distributions can be used to make J^π assignments when they are compared with the shapes of the DWBA calculations, the J^π dependence of the calculations is small so that in many cases the predicted angular distributions for different J^π values cannot be distinguished from one another. In these cases limits on possible J^π values can be assigned. In a few cases, however, spins have previously been restricted to several possible values so that the present data is sufficient to make definite spin assignments.

While the order of the low lying spectra agrees well with the predictions of a weak coupling scheme for an $s_{1/2}$ proton hole coupled to ^{206}Pb (for ^{205}Tl) or ^{204}Pb (for ^{203}Tl), the excitation energies are too small. Furthermore, the large number of high spin states observed (four $\ell=8$ transitions in ^{205}Tl and four $\ell>8$ transitions for ^{203}Tl) cannot be explained in this simple picture. The intermediate coupling scheme⁶ seems far more successful but needs to be extended above 2 MeV excitation. A large shell model investigation of $^{203,205}\text{Tl}$ would also prove most useful in determining the structure of the newly observed high spin transitions. Analysis of the $^{206}\text{Pb}(p,\alpha)^{203}\text{Tl}$ data is still in progress. A study of the $^{204}\text{Pb}(p,\alpha)^{201}\text{Tl}$ reaction is planned.

1. P.A. Smith and R.J. Peterson, Bull. Amer. Phys. Soc. **22** (1977) 1008.
2. R.G. Markham and R.G.H. Robertson, Nucl. Inst. and Meth. **129** (1975) 131.
3. P.A. Smith, W. Weber, G.M. Crawley, and R.G. Markham, MSUCL Annual Report, 1976-1977, p. 25.
4. P.D. Kunz, unpublished.
5. E.R. Flynn, R.E. Anderson, N.J. Diacom, R.J. Peterson, and G.R. Smith, Phys. Rev. C **16** (1977) 139.
6. N. Azziz and A. Covello, Nucl. Phys. **A123** (1969) 681.

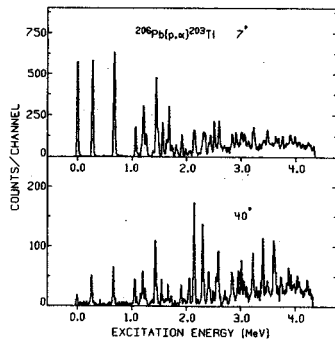


Fig. 1. Spectra of α -particles from the reaction $^{206}\text{Pb}(p, \alpha)^{203}\text{Tl}$ at 7° and 40° .

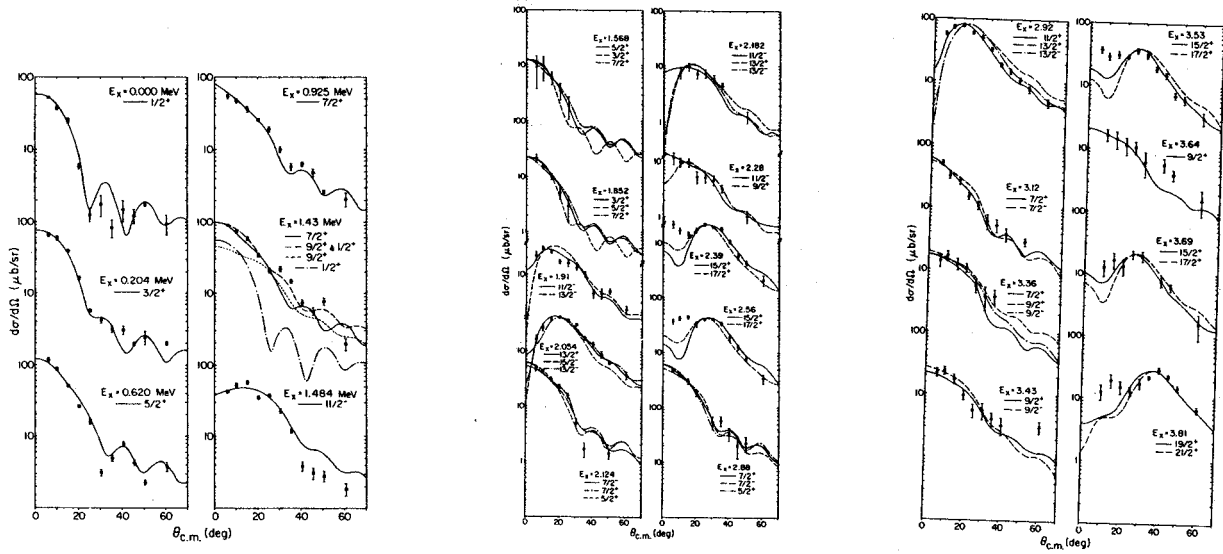


Fig. 2. Angular distributions from the reaction $^{208}\text{Pb}(p, \alpha)^{205}\text{Tl}$.

Shell-Model Predictions for Alpha-Cluster Spectroscopic Factors

W. Chung* and B.H. Wildenthal

The full-space $0d_{5/2} - 1s_{1/2} - 0d_{3/2}$ wave functions of Chung and Wildenthal are being used to calculate spectroscopic factors for alpha-transfer reactions between $16 \leq A \leq 40$ states. The model predictions are obtained by multiplying the matrix element of the 4-nucleon creation operator between the relevant states by factors accounting for the transformation to relative and center of mass coordinates and the overlap of the 4-nucleon cluster from the shell model wave functions with the alpha cluster structure. We assume the leading SU(3) representation for the alpha cluster.

The results of these calculations are being examined in their relationships to alternate calculations as well as to experiment. It appears that the spectroscopic factors are moderately sensitive to both model space and model Hamiltonian specifications. There are some significant disagreements with pure SU(3) predictions. The effects of assuming the pure (8,0) representation for the transferred cluster is also under study. Comparisons with experiment are ambiguous because of the wide scatter in values quoted in the literature. The general trends averaged from experiment are in qualitative agreement with the predictions with the exception that the large increase in experimental strength at ^{40}Ca is not reproduced theoretically.

In Tables 1 and 2 the experimental results of the Rochester group are compared to the present predictions and to results obtained with a pure SU(3) truncation and with Freedom-Wildenthal wave functions. While the theoretical results for ^{24}Mg are rather similar, those for ^{25}Mg exhibit large differences for some excited states.

Table 1. Relative spectroscopic strengths for $^{20}\text{Ne}(^6\text{Li},d)^{24}\text{Mg}$

E_x (MeV)	J^π	$S(^6\text{Li},d)$	$S[\text{SU}(3)]$	$S(\text{PW})$	$S(\text{CW})$
0.0	0^+	1.00	1.00	1.00	1.00
1.37	2^+	0.42	0.37	0.43	0.32
4.12	4^+	0.03	0.00	0.03	<0.01
4.24	2^+	0.13	0.05	0.04	0.09
6.01	4^+	0.28	0.46	0.34	0.46
6.43	0^+	3.87	0.86	0.86	0.83
7.35	2^+	0.37	0.22	0.05	0.17
8.12	6^+	0.09 ± 0.04	0.15	0.00	0.03
8.65	2^+	0.22			0.06

Table 2. Relative spectroscopic strengths for $^{21}\text{Ne}(^6\text{Li},d)^{25}\text{Mg}$

E_x (MeV)	K^π	J	ℓ	$S(^6\text{Li},d)$	$S[\text{SU}(3)]$	$S(\text{PW})$	$S(\text{CW})$
0.00	$5/2^+$	5/2	2	1.00	1.00	1.00	1.00
			4		0.00	0.03	0.04
1.61		7/2	2	1.90	2.20	2.32	1.69
			4		0.04	0.02	0.07
0.58	$1/2^+$	1/2	2	0.24	0.51	0.73	0.02
			0		0.49	1.01	0.43
0.98		3/2	0				
			2	1.94	2.92	5.19	1.77
1.97		5/2	2	1.45	1.28	1.42	0.71
			4		0.01	0.02	0.31
2.74		7/2	2	0.98	0.01	0.23	0.59
			4	1.17	1.32	4.66	2.04
2.56	$1/2^+$	1/2	2	0.37	1.27	0.90	0.99
			0	2.12	0.01	0.15	0.89
2.80		3/2	0				
			2	0.88	0.54	0.01	1.01
3.90		5/2	2	0.42	0.14	0.49	0.22
			4	0.26	2.53	0.13	0.39

*KRA-IKP, Jülich, W. Germany.